NRIAG Journal of Astronomy and Geophysics (2015) **4**, 16–24

National Research Institute of Astronomy and Geophysics

NRIAG Journal of Astronomy and Geophysics

www.elsevier.com/locate/nrjag

REVIEW ARTICLE

Precise troposphere delay model for Egypt, as derived from radiosonde data

M.A. Abdelfatah [a,*], **Ashraf E. Mousa** [b], **Gamal S. El-Fiky** [a]

[a] *Construction Department & Utilities, Faculty of Engineering, Zagazig University, Egypt*
[b] *National Research Institute of Astronomy & Geophysics, Helwan, Egypt*

Received 18 August 2014; revised 8 January 2015; accepted 14 January 2015
Available online 4 March 2015

KEYWORDS

Tropospheric delay;
Radiosonde data;
Troposphere models;
GPS data

Abstract Tropospheric delay computation is necessary to improve GPS measurements accuracy. Precise determination of these propagation delays requires knowledge of the full refraction profile at signal path. In the present research, precise troposphere slant delay model (PTD) is derived based on ten stations of radiosonde data well-distributed over and around Egypt. To derive the PTD, the troposphere is divided into regular small layers. Ray tracing technique of actual signal path traveled in the troposphere is used to estimate tropospheric slant delay.

Real GPS data of six stations in 8-day period were used for the assessment of zenith part of PTD model against the available international models. These international models include Saastamoinen, Hopfield, and the local Egyptian dry model proposed by Mousa & El-Fiky. The data were processed using Bernese software version 5.0. The closure error results indicate that the PTD model is the best model in all session, but when the available radiosonde stations are less, the accuracy of PTD model is near to classic models. As radiosonde data for all ten stations are not available every session, it is recommended to use one of the regularization techniques for database to overcome missing data and derive consistent tropospheric delay information.

* Corresponding author.
Peer review under responsibility of National Research Institute of Astronomy and Geophysics.

Production and hosting by Elsevier

http://dx.doi.org/10.1016/j.nrjag.2015.01.002

Contents

1. Introduction

Troposphere is the lower part of atmosphere near to earth's surface and ranges up to 16 km in altitude (e.g. Kleijer, 2004). The Troposphere affects the GPS signals significantly since the signals are both delayed and refracted (e.g. Mousa and El-Fiky, 2005). The main factors which cause troposphere delay include temperature, pressure, and humidity. The delay also varies with the height of the user position as the type of terrain below the signal path can affect the delay (Musa et al., 2011). There are two components of troposphere delay, namely wet delay and dry delay. The dry component which comprises about 80–90% of the total delay is easier to determine as compared to the wet component (e.g. Abdelfatah et al., 2009).

Mathematically the tropospheric delay Δ^{Trp} can be represented as

$$\Delta^{Trp} = 10^{-6}\int_s Nds + (S - G) \tag{1}$$

where N is the group refractivity along the path taken by the ray of signal (denoted by S in the integral), and G is defined as the geometric path in meters. The integration is along the actual path traveled S. The integral part of the above equation is the refractivity error while the term $(S - G)$ is the geometric range error in meters (Fig. 1).

Refractivity of the air (N) is given by (Kleijer, 2004; Mousa and El-Fiky, 2005)

$$N = k_1\frac{P_d}{T}Z_d^{-1} + k_2\frac{e}{T}Z_w^{-1} + k_3\frac{e}{T^2}Z_w^{-1} \tag{2}$$

where P_d is the dry atmospheric pressure in mbar, e is the water vapor pressure in mbar, T is the temperature in Kelvins. The constant parameters are $k_1 = 77.6$ K/mbar, $k_2 = 71.6$ K^2/mbar and $k_3 = 3.747\times10^5$ K^2/mbar. Z_d and Z_w are the compressibility factors for the dry component and water vapor, respectively.

GPS satellite positioning is based upon transmitted electromagnetic waves from the satellite to the user on the ground. A

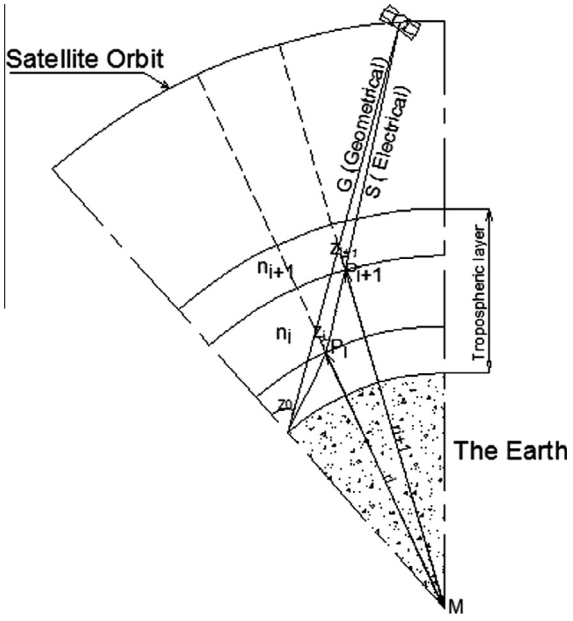

Fig. 1 Schematic ray path of signal for space geodetic measurement (e.g. Kleijer, 2004).

radio signal passing through the earth's atmosphere suffers a change in direction owing to atmospheric refraction (e.g. Musa et al., 2011). The total change of path direction can be found by repeatedly applying Snell's law for each layer of the atmosphere.

The mathematical formulation of Snell's law in spherical coordinates for a spherical earth with a spherically layered atmosphere may be derived by application of the sine rule in the triangle $M\ P_i\ P_{i+1}$ of Fig. 1. This gives (Kleijer, 2004)

$$n_{i+1}r_{i+1}\sin z_{i+1} = n_i r_i \sin z_i = n_0 r_0 \sin z_0 \tag{3}$$

where r_i and r_{i+1}, in meters, are the distances MP_i and MP_{i+1}, with M the center of mass of the earth and $r_{i+1} = r_i +$ thick-

ness of layer and n is group refractive index ($n = 1 + N \cdot 10^{-6}$).

During the last several years, a number of models (Hopfield model, Saastamoinen model, Mousa and El-Fiky model, etc.) have been developed and reported in scientific literature by researchers for estimation and correction of the delay induced by the troposphere in the GPS signal. However, much research has gone into the creation and testing of tropospheric refraction models to compute the refractivity (N) along the signal traveled path.

In the present research, we develop a new model called as the precise troposphere delay model (PTD). This model is derived by solving the integration equation (Eq. (1)) in slant direction using ten stations of radiosonde data well-distributed all over Egypt. Radiosonde is the balloon-borne instrument package that sends temperature, humidity, and pressure data to the ground by radio signal (Musa et al., 2011). Radiosonde data are one of the most used and precise techniques to derive the atmospheric vertical profile (Wyoming, 2013). Real GPS data of six stations in 8-day period are used for the assessment of zenith part of PTD model against the available international models.

2. Tropospheric models

In GPS applications, the tropospheric delay is handled by means of global tropospheric delay models based on climate data. Some models are explicitly dependent on surface meteorological data and others use the coordinates (latitude and height) of the GPS station. Abdelfatah et al. (2009) carried out an assessment of tropospheric delay models and recommended Saastamoinen and Hopfield model for Egypt. Mousa and El-Fiky (2005) have developed a local model for Egypt. The three tropospheric models give the best results for Egypt and thus are used here for the assessment of the new PTD model. These three models are described in the following paragraphs.

2.1. The Saastamoinen model

The standard model of Saastamoinen (1973) is normally used to compute the dry tropospheric delay given the surface pressure information. Saastamoinen model expresses the Tropospheric delay (Δ^{Trp}) in meters as

$$\Delta^{Trp} = \frac{0.00277}{\cos z}\left[P + \left(\frac{1255}{T} + 0.05\right)e + B\tan^2 z\right] + \delta R \qquad (4)$$

where P is the total surface pressure in mbar, e the partial water surface pressure in mbar, T the surface temperature in degrees Kelvin and B & δR are correction terms that depend on the height and zenith of the observing site, respectively. Saastamoinen model has vertical accuracy of about 6.2 mm (Abdelfatah et al., 2009).

2.2. Hopfield model

Hopfield assumes a spherical earth and that the temperature decreases linearly with increasing height in the troposphere (Hopfield, 1971), but the temperature remains constant in the stratosphere (the second layer of the atmosphere)

$$\Delta^{Trp} = \Delta d + \Delta w \qquad (5)$$

where Δd is zenith hydrostatic path delay and Δw is zenith wet path delay

$$\Delta d = 15.528\frac{P}{T}\frac{(h_d - h_s)^5}{h_d^4} \times 10^{-6} \qquad (6a)$$

$$\Delta w = 74600\frac{e}{T^2}h_w \times 10^{-6} \qquad (6b)$$

where P, T and e are the same parameters as Saastamoinen model, and h_d, h_w are the dry and the wet atmosphere heights respectively in meters, and h_s is the station height in meters. Accuracy of Hopfield model is in the same range as Saastamoinen model (Abdelfatah et al., 2009).

To determine the delay at any desired elevation angle, a model is used to map the zenith delay to that elevation angle. This model is known as mapping function. Using the same assumptions used by Saastamoinen (1973) in deriving his mapping function, Goad and Goodman (1974) have solved the integration of Eq. (1) based on a series expansion of the integrand to give the mapping function as

$$MF_i = \frac{5}{h_i - h_s} \pm \sum_{k-1}^{9} f_{i,k}\frac{r_i^k}{k} \qquad (7)$$

where $f_{i,k}$ are the mapping function parameters and the subscript "i" refers to either the dry or the wet component and k is an integer number from 1 to 9.

2.3. Mousa & El-Fiky model

Mousa and El-Fiky (2005) developed a model to calculate hydrostatic zenith path delay using metrological data from ten stations distributed all over Egypt. This model takes the form

$$\Delta^{Trp} = a + b \times P \qquad (8)$$

where a and b are constant parameters and P is surface pressure.

All available tropospheric models do not consider anti-symmetric of troposphere and neglect geometric delay. Saastamoinen showed that the atmospheric constituents are in hydrostatic equilibrium; thus, the delay can be determined by measuring the surface pressure. However to achieve better accuracy, it is needed to consider the whole vertical profile of the atmosphere (e.g. Abdelfatah et al., 2009). Hopfield assumed a spherical Earth and used surface metrological data but the shape of Earth is nearly an ellipsoid and the troposphere shape is changing with time. Besides the signal curvature is neglected. Mousa and El-Fiky model considered only hydrostatic zenith delay; they used linear regression to estimate the terms "a" and "b" in Eq. (8). As a result, the term "a" does not equal 0 which means that if the pressure equals zero the delay will not equal zero. Therefore a new model is still needed for use with GPS data in Egypt which is the main aim of this paper.

3. PTD model derivation steps

The calculation of the PTD is implemented in six main steps. In the first step, the available radiosonde data from the ten

stations are collected and used to calculate the refractivity as a function of height as is explained below. In the next step, we make height regularization by assuming that the atmosphere consists of co-centric layers with the earth center as the common center. Each layer is of 50 m thickness, and the values of refractivity are calculated at this regular height steps. In the third step, surfaces are fitted to provide the refractivity at any location (Φ, λ) at any specified atmospheric layer.

To carry out the integral in Eq. (1), we need to determine the length (ds). To calculate this length, the atmosphere is divided into concentric layers with 50 m thickness. For every ray connecting the satellite to receiver (at all possible azimuth), the ray intersection points coordinates with the boundary of each atmospheric layer are estimated. To calculate the above intersection points, we derived the ray equation inside each layer. Then the equation is solved with the atmosphere boundaries layer taking into account the refraction of the ray between layers as given below. In the last step, the distance (length of the ray at any layer) is calculated as the distance between the above intersection points.

A visual C.net subroutine was developed to estimate the PTD values. Fig. 2 illustrates the main steps of the software implementation. In the following sections, the detailed mathematical manipulation of each of the six steps is discussed in more detail along with a basic mathematical treatment of these steps.

3.1. Radiosonde database

The department of atmospheric sciences of University of Wyoming has a radiosonde database for the whole world. It includes ten radiosonde stations distributed in and around Egypt (Fig. 3). Stations name, and its approximate coordinates are given also in Table 1. The soundings are available on http://weather.uwyo.edu/upperair/sounding.html. The needed data for modeling the PTD are height (H) in meter, P in mbar, T in °C and mixing ratio ($MixR$) in gram/kilogram (Wyoming, 2013).

3.2. Step 1: calculation of refractivity

Using the sounding parameter (P, T, $MixR$, and H), dry pressure (P_d) and wet vapor pressure (e) can be calculated through the following equations:

$$e_{k,i} = \frac{P_{k,i} \cdot MixR_{k,i}}{MixR_{k,i} + 622} \tag{9}$$

$$P_{dk,i} = P_{k,i} - e_{k,i} \tag{10}$$

where the subscript k is radiosonde station name and i is the layer of the measured data in radiosonde station.

Now we can calculate N as a function of the height using Eq. (2).

3.3. Step 2: radiosonde height realization

The data of radiosonde are not at a uniform height so Lagrange interpolation is used to predict N' at a uniform value of H' (0, 50, 100…). Four points were used such that two points have values greater than the predicted point and the other two points have values lower than the predicted point. The initial and last values could be linearly extrapolated. First, we determine the maximum height of each radiosonde station. This height is calculated such that the value refractivity equals zero. H'_F is the stopping point of integration of equation (1).

$$H'_F = \left[H_g - \frac{H_{g-1} - H_g}{N_{g-1} - N_g} N_g \right] \tag{11}$$

where H_g and N_g are the end value of height and reflection in radiosonde data, H_{g-1} and N_{g-1} are the pre-end value of height and reflection, and H'_F is the height up to zero reflection.

Now number of atmospheric layer (no) can be determined as

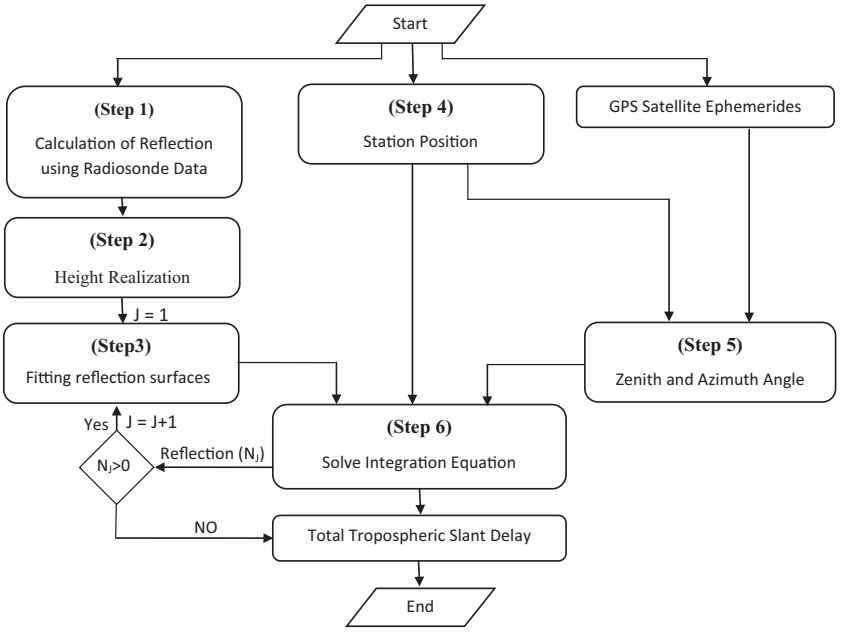

Fig. 2 Main steps of the software of PTD implementation.

Fig. 3 Radiosonde stations used in the present study.

Table 1 Approximate coordinates of the GPS stations and radiosonde stations.

Station code	Station type	Latitude (°)	Longitude (°)
ABSM	GPS	22.49	31.54
ARSH		31.11	33.62
ASWN		23.97	32.85
MTRH		31.35	27.23
PHLW		29.86	31.34
SALU		31.49	25.21
40179	Radiosonde	32.00	34.81
40375		28.38	36.60
40430		24.55	39.70
41024		21.70	39.18
62306		31.33	27.21
62337		31.08	33.81
62378		29.86	31.33
62423		27.05	27.96
62403		26.20	32.75
62414		23.96	32.78

$$n_o \cong \frac{H'_F}{50} \tag{12}$$

It is often convenient to use simple discontinuous function (the unit step function). We will use the notation U (.) to denote this function, and define it as

$$U(x) = 0 \text{ for } x < 0 \text{ and } U(x) = 1 \text{ for } x \geq 0.$$

Using the unit step function, it is possible to define a "stair-step" function as a summation. In particular, the cumulative distributions function for a discrete random variable such as that given in the following equation:

$$\begin{aligned}
&\left[N_1 + \frac{N_2 - N_1}{H_2 - H_1}(H'_j - H_1)\right] U(H'_j - H_2) + N'_j \\
&= \sum_{i=1}^{n_o} \left[\frac{(H'_j - H_{i-1})(H'_j - H_i)(H'_j - H_{i+1})}{(H_{i-2} - H_{i-1})(H_{i-2} - H_i)(H_{i-2} - H_{i+1})} N_{i-2} \right. \\
&\quad + \frac{(H'_j - H_{i-2})(H'_j - H_i)(H'_j - H_{i+1})}{(H_{i-1} - H_{i-2})(H_{i-1} - H_i)(H_{i-1} - H_{i+1})} N_{i-1} \\
&\quad + \frac{(H'_j - H_{i-2})(H'_j - H_{i-1})(H'_j - H_{i+1})}{(H_i - H_{i-2})(H_i - H_{i-1})(H_i - H_{i+1})} N_i \\
&\quad \left. + \frac{(H'_j - H_{i-2})(H'_j - H_{i-1})(H'_j - H_i)}{(H_{i+1} - H_{i-2})(H_{i+1} - H_{i-1})(H_{i+1} - H_i)} N_{i+1} \right] \\
&\quad \times [U(H_{i-1} - H'_j) - U(H_i - H'_j)] \\
&\quad + \left[N_{n_o-1} + \frac{N_{n_o-1} - N_{n_o}}{H_{n_o-1} - H_{n_o}}(H'_j - H_{n_o})\right] U(H_{n_o-1} - H'_j)
\end{aligned} \tag{13}$$

This equation can be written as $f(N'j) = H'j$ where j is from 1 to the number of layers (n_o).

3.4. Step 3: refractivity surfaces fitting

At each height, to calculate the refractivity at any desired location (Φ, λ) a surface is fitted to the refractivity using the ten points from radiosonde after calculated refraction.

First, geodetic coordinate (Φ, λ) is converted to Cartesian coordinate (X_e, Y_e, Z_e) using following matrix (e.g. Molnár and Timár, 2005):

$$\begin{bmatrix} X_{e_j} \\ Y_{e_j} \\ Z_{e_j} \end{bmatrix} = \begin{bmatrix} (N_{e_j} + N_j)\cos\lambda \cdot \cos\Phi \\ (N_{e_j} + N_j)\sin\lambda \cdot \cos\Phi \\ (N_{e_j}(1 - e^2_{e_j}) + N_j)\sin\Phi \end{bmatrix} \tag{14}$$

where a_e is the ellipsoid semi major axis, e_e is the first eccentricity and N_e is normal radii of curvature. The above equation

gives the coordinate X_e, Y_e, Z_e for a point at a certain height. The total number of raw $= 3 \times j$, the subscript j is the same as in Eq. (11).

For each radiosonde station with equal value of H', we could fit a surface (of the refractivity) of two parameters ($P1$, $P2$) using least squares such that

$$(X_e^2 + Y_e^2) \times P1 + (Z_e^2) \times P2 - 1 = V \tag{15a}$$

where V is vector holding all residuals. The un-weighted least squares solution is given by

$$V = A \cdot Pa - L \tag{15b}$$

where A is the design (coefficient) matrix, Pa is a vector which contains the unknown parameters, and L is the observations.

$$V = \begin{bmatrix} V_1 \\ V_2 \\ V_3 \\ \\ V_j \end{bmatrix} = \begin{bmatrix} (x_{e1}^2 + y_{e1}^2) & z_{e1}^2 \\ (x_{e2}^2 + y_{e2}^2) & z_{e2}^2 \\ (x_{e3}^2 + y_{e3}^2) & z_{e3}^2 \\ \\ (x_{ej}^2 + y_{ej}^2) & z_{ej}^2 \end{bmatrix} \cdot \begin{bmatrix} P_1 \\ P_2 \end{bmatrix} - \begin{bmatrix} 1 \\ 1 \\ 1 \\ \\ 1 \end{bmatrix} \tag{15c}$$

Employing the least squares principle with $V^T PV =$ a minimum leads to the normal equations

$$Pa = (A^T A)^{-1} A^T L \tag{16}$$

3.5. Step 4: equation of slant ray in three dimensions coordinates

At any station, Z: Zenith angle, α: azimuth angle. Equation of slant signal ray in local coordinate is given as

$$\begin{bmatrix} \hat{u} \\ \hat{v} \\ \hat{w} \end{bmatrix} = \begin{bmatrix} \sin z \cdot \cos \alpha \\ \sin z \cdot \sin \alpha \cdot \cos \lambda \\ \cos z \end{bmatrix} \tag{17}$$

where $\hat{u}, \hat{v}, \hat{w}$ are unit vectors of the slant line.

$$\begin{bmatrix} a \\ b \\ c \end{bmatrix} = \begin{bmatrix} -\sin z \cdot \cos \alpha \cdot \sin \Phi \cdot \cos \lambda - \sin z \cdot \sin \alpha \cdot \sin \lambda + \cos z \cdot \cos \Phi \cdot \cos \lambda \\ -\sin z \cdot \cos \alpha \cdot \sin \Phi \cdot \sin \lambda + \sin z \cdot \sin \alpha \cdot \cos \lambda + \cos z \cdot \cos \Phi \cdot \sin \lambda \\ \sin z \cdot \cos \alpha \cdot \cos \Phi + 0 + \cos z \cdot \sin \Phi \end{bmatrix} \tag{18}$$

where a, b, c are components of a vector in the direction of the line ('slope' or 'orientation').

3.6. Step 5: get Cartesian, geodetic coordinate and zenith angle of the next layer

By solving equation of surface (Eq. (15)) with Eq. (18), we get

$$\begin{bmatrix} a' \\ b \\ c' \end{bmatrix} = \begin{bmatrix} P1 \cdot (a^2 + b^2) + P2 \cdot c^2 \\ 2P1(a \cdot x_{ej} + b \cdot y_{ej}) + 2P2 \cdot c \cdot z_{ej} \\ P1(x_{ej}^2 + y_{ej}^2) + P2 \cdot z_{ej}^2 - 1 \end{bmatrix} \tag{19}$$

where a', b', c' are components of a distance between the intersection point and the next surface. Then, substituting the following equation (Eq. (20)) into Eq. (18) yields: X_{ej+1}, Y_{ej+1}, Z_{ej+1} in the Eq. (21) form

$$t = \frac{-b' + \sqrt{b'^2 - 4a'.c'}}{2a'} \tag{20}$$

$$\begin{bmatrix} X_{ej+1} \\ Y_{ej+1} \\ Z_{ej+1} \end{bmatrix} = \begin{bmatrix} a \\ b \\ c \end{bmatrix} \cdot t + \begin{bmatrix} X_{ej} \\ Y_{ej} \\ Z_{ej} \end{bmatrix} \tag{21}$$

where t is called a parameter that can be any real number. X_{ej}, Y_{ej}, Z_{ej} are coordinate of point passes through the line and X_{ej+1}, Y_{ej+1}, Z_{ej+1} coordinate of intersection point between line and surface.

After solving the equation of slant line we get X_{ej+1}, Y_{ej+1}, Z_{ej+1}. However, the geodetic coordinates are required to calculate equation of ray segment in the next layer. Older textbooks and manuals give equations for the Molodensky transformation (e.g. Molnár and Timár, 2005) that would be used. These give directly the shifts in latitude and longitude. These formulas will be given here for completeness. The standard form is often given as

$$\begin{bmatrix} \Phi_{j+1} \\ \lambda_{j+1} \end{bmatrix} = \begin{bmatrix} \frac{\sin \Phi_j \cdot \cos \lambda_j}{ae_j} & \frac{\sin \Phi_j \cdot \sin \lambda_j}{ae_j} & \frac{-\cos \Phi_j}{ae_j} \\ \frac{\sin \lambda_j}{ae_j} & \frac{-\cos \lambda_j}{ae_j} & 0 \end{bmatrix} \times \begin{bmatrix} \Delta x_j \\ \Delta y_j \\ \Delta z_j \end{bmatrix} + \begin{bmatrix} \Phi_j \\ \lambda_j \end{bmatrix} \tag{22}$$

where $(\Phi_{j+1}, \lambda_{j+1})$ is the geodetic coordinate of the next reflection layer, a_e is the ellipsoid semi major axis and $(\Delta x_j, \Delta y_j, \Delta z_j)$ are (datum shift parameters) different between Cartesian coordinate of the layer (j) and next layer ($j + 1$).

The radius of the earth is very big relative to atmospheric height so we can assume that

$$\frac{R_i}{R_{i+1}} = \frac{R_i}{R_i + \Delta H} = \frac{1}{1 + \frac{\Delta H}{R_i}} = 1 - \frac{\Delta H}{R_i} = 1 - \frac{\Delta H}{a.\frac{\sqrt{(1-e^2)}}{1-e^2 \cdot \sin \Phi^2}} \tag{23}$$

The zenith angle in the next layer is calculated by Substituting Eqs. (22) and (23) into Eq. (3). This yields (Fig. 1)

$$Z_{i+1} = \sin^{-1}\left[\left(1 - \frac{\Delta H}{a \cdot \frac{\sqrt{(1-e^2)}}{1-e^2 \cdot \sin \Phi^2}}\right) \times \left(\frac{1 + N_{i-1} \cdot 10^{-6}}{1 + N_i \cdot 10^{-6}}\right) \times \sin(Z_i)\right] \tag{24}$$

3.7. Step 6: calculate slant delay

By using coordinates of two interval intersection points (Eq. (21)), we get slant distance ΔS and troposphere errors as follows:

$$\Delta S = \sqrt{(X_{ej+1} - X_{ej})^2 + (Y_{ej+1} - Y_{ej})^2 + (Z_{ej+1} - Z_{ej})^2} \tag{25}$$

$$\text{Troposphere error} = \sum_1^J \frac{N_{i-1} + N_i}{2} \Delta S \tag{26}$$

Fig. 4 The six permanent GPS stations of NRIAG used in this study.

Table 2 GPS baseline loops and radiosonde stations used.

Session	Date	Radiosonde stations codes	GPS stations loop
Mid-day	02/01/2013	40179, 40375, 40430,41024, 62423	ASWN, MTRH, PHLW
	03/05/2013	40179, 40375, 41024, 62403, 62414, 62423	ABSM, ARSH, SALU
	11/09/2013	40179, 40375, 40430, 41024, 62337, 62403, 62414	ARSH, ASWN, MTRH
	01/12/2013	40179, 40430, 41024, 62337, 62378, 62403	ARSH, MTRH, PHLW
Mid night	10/10/2013	40179, 40375, 40430, 41024, 62378, 62414	ASWN, MTRH, PHLW
	21/04/2013	40179, 40430, 62337, 62414	ABSM, ARSH, PHLW
	03/07/2013	40179, 40375, 40430, 41024, 62337, 62378, 62414	ARSH, ASWN, MTRH
	03/02/2013	40179, 40430, 41024, 62337, 62414	ARSH, MTRH, PHLW

The final model PTD was driven as a function of the parameters α, ze, Φ, λ, H, and radiosonde data.

4. Data analysis

To test the PTD model, six GPS stations of the National Research Institute of Astronomy and Geophysics (NRIAG) permanent stations are used here (Fig. 4). Stations name, type and its approximate coordinates are listed in Table 1. The GPS observations were carried out using Trimble NETR5 receivers. GPS stations data were processed as baselines. In the present research we only tested zenith path delay using Niell mapping function model (Niell, 1996). It is meanwhile to mention that the model of Mousa & El-Fiky has no wet delay so we added the wet part of the PTD model to hydrostatic term of Mousa & El-Fiky model.

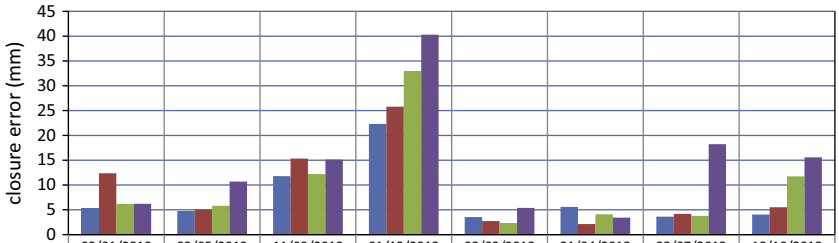

	02/01/2013 Day session	03/05/2013 Day session	11/09/2013 Day session	01/12/2013 Day session	03/02/2013 Night session	21/04/2013 Night session	03/07/2013 Night session	10/10/2013 Night session
PTD	5.3	4.8	11.8	22.3	3.5	5.6	3.6	4.0
E & M	12.4	5.1	15.3	25.8	2.7	2.1	4.2	5.5
Hop	6.2	5.8	12.2	33.0	2.3	4.1	3.8	11.7
Saa	6.2	10.7	15.1	40.3	5.4	3.4	18.2	15.6

Fig. 5 GPS baseline closure error (mm). Here E & M, Hop, and Saa stand for Mousa and El-Fiky, Hopfield, and Saastamoinen models, respectively.

A closed triangle formed by three GPS baselines is used to test the zenith path delay effect and closure error. The GPS-EST program of Bernese GPS software version 5 (Dach et al., 2007) is used to test models of troposphere delay for baselines closure error. Table 2 depicts the GPS loop stations names and radiosonde stations codes.

5. Results and discussion

Fig. 5 presents the temporal variations of the closure errors of the PTD model and the other classic models over the 8-days period. Eight sessions were selected out from the observed baselines for the GPS network. The selected sessions covered all possible cases: (winter, spring, summer, and autumn), as well as day and night sessions.

In contrast, the closure errors during the most seasons of classic model show a good agreement with the PTD Model. In day session, we selected four campaigns. The PTD model is the best model in all seasons; however, Mousa and El-Fiky (2005) model has very close results to it in all seasons except the winter (02/01/2013). Hopfield model has accuracy better than Saastamoinen model in the summer (11/09/2013) and the autumn (01/12/2013) seasons. But generally these seasons show high values of the closure errors.

In night session, we selected four campaigns as shown in Fig. 5. The PTD model is the best model in summer (03/07/2013) and autumn (10/10/2013) seasons; however, Mousa and El-Fiky (2005) model has very close results to it in all seasons. Hopfield model has accuracy better than Saastamoinen model in all seasons except spring (21/04/2013) season.

The results indicate that the developed PTD model is superior to the existing tropospheric models in all sessions except in April and February sessions. This might be due to the limited available number of radiosonde stations. Generally, the closure errors in the day sessions are greater than night session. It is noticeable that the greatest closure errors are shown in the autumn season. The closure errors of PTD model in December session reached to 22.3 mm which is greater than one of summer sessions, although the summer season that had the greatest temperature. This could be due to different limited number of radio stations used in autumn (six stations) compared with that used in summer (seven stations).

In the most sessions, Saastamoinen model shows low accuracy. The closure errors of PTD model are near to that of Mousa & El-Fikly model in the most session. This might be due to both have the same wet part of delay. On the other side, Hopfield model is better than Saastamoinen model in most of the sessions. It is important to mention here that there is no session containing ten radiosonde stations fully. So we might conclude that by increasing number of radiosonde stations some improvement could be reached in the adjusted results. Finally, to improve the present PTD model introduced in the present study, database and predicted model to overcome inadequate radiosonde data are urgently needed.

6. Conclusions

In the present research, a new precise troposphere slant delay model (PTD) is introduced. The model is based on a ray tracing technique for estimating the tropospheric delay using radiosonde records. Ten stations distributed in and around Egypt are used as the input radiosonde data for the model calculation. The new model takes into account geometric delays as well as atmospheric asymmetry. The model gives the slant path delay directly without any need for a mapping function. Due to the available data, only zenith value of the new model is tested here.

Six GPS stations are used to test the new model performance. When the radiosonde data were available at all used ten stations, the test results indicate that PTD model shows the best performance, compared to Saastamoinen, Hopfield, and Mousa and El-Fiky models. However, if the radiosonde data were not available at some stations, the results of PTD model are very near to other classic models. In case of radiosonde data that are available, the new model provides good result and it is recommended to be used when processing GPS data in order to get high accuracy results.

Further studies should be carried out to overcome the missing data of radiosonde using one of the regularization techniques for database.

Acknowledgments

The authors are grateful to the staff of geodynamic department of the National Research Institute of Astronomy and Geophysics, Helwan, Cairo, who participated in the GPS data used in this study and for allowing me to use their licensed Bernese GPS software version 5.

References

Abdelfatah, M.A., Mousa, A.E., Salama, I.M., El-Fiky, G.S., 2009. Assessment of tropospheric delay models in GPS baseline data analysis: a case study of a regional network at upper Egypt. J. Civil Eng. Res. Mag. AL-Azhar Univ. 31 (4), 1143–1156.

Dach, R., Hugentobler, U., Fridez, P., Meindl, M., 2007. User Manual of the Bernese GPS Software Version 5.0. Astronomical Institute, University of Bern.

Hopfield, H.S., 1971. Tropospheric effect on electromagnetically measured range: prediction from surface weather data. Radio Sci. 6, 357–367.

Goad, C.C., Goodman, L., 1974. A modified Hopfield tropospheric refraction correction model. In: AGU Anual Fall meeting.

Kleijer, F., 2004. Troposphere Modeling and Filtering for Precise GPS Leveling. Delft University of Technology, Netherlands Geodetic Commission.

Molnár, G., Timár, G., 2005. Determination of the parameters of the abridging Molodensky formulae providing the best horizontal fit. Geophys. Res. Abstracts 7, 01018 (2005SRef-ID: 1607-7962/gra/EGU05-A-01018).

Mousa, A.E., El-Fiky, G.S., 2005. A proposed local dry zenith delay model for GPS measurements in Egypt, as derived from surface pressure data. J. Sci. Bullet. 40 (1), 361–371.

Musa, T.A., Musa, N., Amir, S., Othman, R., Ses, S., Omar, K., Abdullah, K., Lim, S., Rizos, C., 2011. GPS meteorology in a low-latitude region: remote sensing of atmospheric water vapor over the Malaysian Peninsula. J. Atmosp. Solar-Terrest. Phys. 73, 2410–2422.

Niell, A.E., 1996. Global mapping functions for the atmosphere delay at radio wavelengths. J. Geophys. Res. 101 (B2), 3227–3246.

Saastamoinen, J., 1973. Contribution to the theory of atmospheric refraction. Bullet. Geodesique 107, 13–34.

Wyoming Dep. of Atmospheric Science, 2013. <http://weather.uwyo.edu/upperair/sounding.html> (accessed June 2013).